Electronic Supporting Information (ESI) for

Grafting density and antifouling properties of poly[*N*-(2-hydroxypropyl) methacrylamide] brushes prepared by "grafting to" and "grafting from"

*Yu-Min Wang,[ab] Anna Kálosi,[cd] Yuriy Halahovets,[d] Iryna Romanenko,[ab] Jiří Slabý,[e] Jiří Homola,[e] Jan Svoboda,[a] Andres de los Santos Pereira [*a] and Ognen Pop-Georgievski [*a]*

[a]Institute of Macromolecular Chemistry, Czech Academy of Sciences, Heyrovský sq. 2, 16206 Prague, Czech Republic

[b]Department of Physical and Macromolecular Chemistry, Charles University, Hlavova 8, 12800 Prague, Czech Republic

[c]Centre for Advanced Material Application, Slovak Academy of Sciences, Dúbravská cesta 9, 84511 Bratislava, Slovakia

[d]Department of Multilayers and Nanostructures, Institute of Physics, Slovak Academy of Sciences, Dúbravská cesta 9, 84511 Bratislava, Slovakia

[e]Institute of Photonics and Electronics, Czech Academy of Sciences, Chaberská 1014/57, 18251 Prague, Czech Republic

*corresponding authors: santospereira@imc.cas.cz, georgievski@imc.cas.cz

In situ ellipsometry

In situ ellipsometry data were acquired using an in-house developed variable AOI immersion cell/cuvette operating in water. The cell/cuvette is comprised of immersion dish filled with liquid/environment of interest and two optically flat plates (strain-free, ϕ = 5 mm and h = 2 mm, UV fused silica from UQG-Optics, Great Britain), serving as entrance and exit windows which are immersed in the liquid of interest. The windows are connected rigidly to the polarizer and analyzer ellipsometer arms and lack any contact with the immersion dish and sample, thus providing measurements at various AOI. The windows are orthogonal to the beam, thus attaining perfect orientation of the beam in air and in liquid environment. This completely avoids errors in the goniometer set AOI caused by the windows presence. The minimal optical retardation of the windows was measured in a straight-through configuration, i.e. AOI = 90°. All measurements were corrected for the windows' in-plane retardance effects on ellipsometric angle Δ according the relation:

$$\Delta_{Offsets}(\lambda) = \Delta_{Offset\,1} + \frac{\Delta_{Offset\,2} \times \lambda^2}{100}$$

The values of $\Delta_{\text{Offset 1}}$ and $\Delta_{\text{Offset 2}}$ were determined to be -0.011 ± 0.001 and 0.021 ± 0.004, respectively within the wavelength range (Fig. S1). The Ψ_{Offsets} due presence of windows was not considered because values were within the precision of ellipsometric measurement in a straight-through configuration i.e. 45.000° ± 0.075°. The obtained data were fitted with CompleteEASE software using a multilayer model. We have utilized the multiple environment approach (MEA) to determine the optical dispersion function of the gold layers. Ellipsometric data of bare samples in air and water were treated with basis spline function having the complex refractive index of

single crystal gold as a seeding value at each measured wavelength. As the optical properties of gold are independent on the environment in which the measurement has been performed, we gain more analytical/fitting power in additional data oversaturation of the models and in this way obtaining more reliable results for the complex refractive index of gold. (Note: In addition to the in situ measurement at multiple AOI, the MEA for determining the substrate's dispersion function is another prerequisite to obtain reliable ellipsometric data/results for the swollen layers). The optical dispersion function of water was taken from the CompleteEase database. The thickness and refractive index of the dry and swollen poly(HPMA) layers were obtained from simultaneous fitting of the obtained ellipsometric data using Cauchy dispersion functions:

$$n = A + \frac{B}{\lambda^2} + \frac{C}{\lambda^4}$$

All reported values are averages obtained of 3 independent samples, expressed as mean ± standard deviation.

Calculation of water content in swollen poly(HPMA) layers and consistency of ellipsometric results

Thicknesses determined by ellipsometry in dry and swollen state were used to calculate the swelling ratio according:

$$Swelling\ ratio = \frac{h_{swollen}}{h_{dry}}$$

The volume fraction of water (*f*) inside the poly(HPMA) layers was determined by:

$$f_h = \frac{h_{swollen} - h_{dry}}{h_{swollen}}$$

$$f_{L-L\,EMA} = \frac{\left(\frac{n_{swollen}^2 - n_{dry}^2}{n_{swollen}^2 + 2n_{dry}^2}\right)}{\left(\frac{n_{H2O}^2 - n_{dry}^2}{n_{H2O}^2 + 2n_{dry}^2}\right)}$$

where f_h is the volume fraction calculated from the poly(HPMA) layer thicknesses in swollen $h_{swollen}$ and dry h_{dry} state, $f_{L-L\,EMA}$ is the volume fraction of water calculated by Lorentz-Lorenz effective medium approximation (EMA) from the refractive indices of water (n_{H2O}), dry (n_{dry}) and swollen ($n_{swollen}$) poly(HPMA) layers. The close matching of calculated volume fractions (Table S1) points to the low correlation of the model-derived thicknesses and corresponding optical dispersion functions and their consistency.

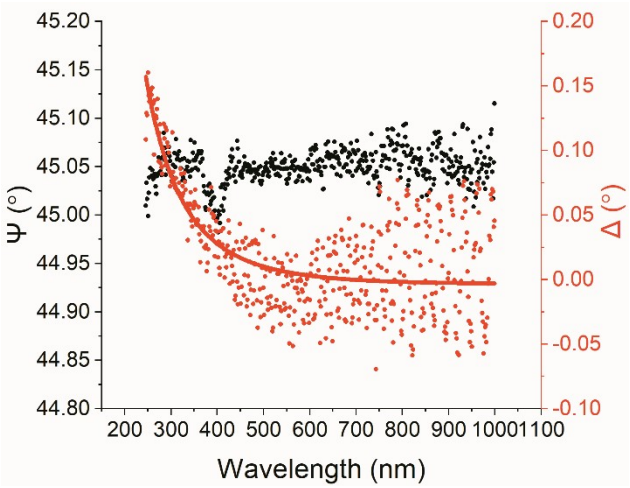

Fig. S1. Window retardance effects on ellipsometric angles Ψ and Δ determined in straight-through configuration. Measured Δ_{offset} (points) were modelled (lines) according the elaborated dispersion relation.

Table S1. Cauchy optical dispersion functions of poly(HPMA) brushes in dry and swollen state. Corresponding water volume fractions f_h and $f_{L-L\,EMA}$ were calculated to estimate the consistency of data.

	Dry brushes			**Swollen brushes**			**Water volume fraction**	
Poly(HPMA) Brush layer	$A_{n\ \mathrm{dry}}$	$B_{n\ \mathrm{dry}}$ (nm^{-2})	$C_{n\ \mathrm{dry}}$ (nm^{-4})	$A_{n\ \mathrm{swollen}}$	$B_{n\ \mathrm{swollen}}$ (nm^{-2})	$C_{n\ \mathrm{swollen}}$ (nm^{-4})	f_h	$f_{L-L\,EMA}$
GT-SG	1.4731 ± 0.0080	5314 ± 886	1.20×10^{8} ± 2.58×10^{6}	1.3477 ± 0.0045	100 ± 15	1.43×10^{8} ± 1.71×10^{6}	0.85 ± 0.01	0.93 ± 0.02
GT-PS				1.3697 ± 0.0040	569 ± 10	1.20×10^{8} ± 3.69×10^{6}	0.77 ± 0.02	0.80 ± 0.03
GF				1.4130 ± 0.0014	3840 ± 560	5.24×10^{7} ± 3.09×10^{7}	0.53 ± 0.02	0.51 ± 0.01

AFM topography of the poly(HPMA) layers

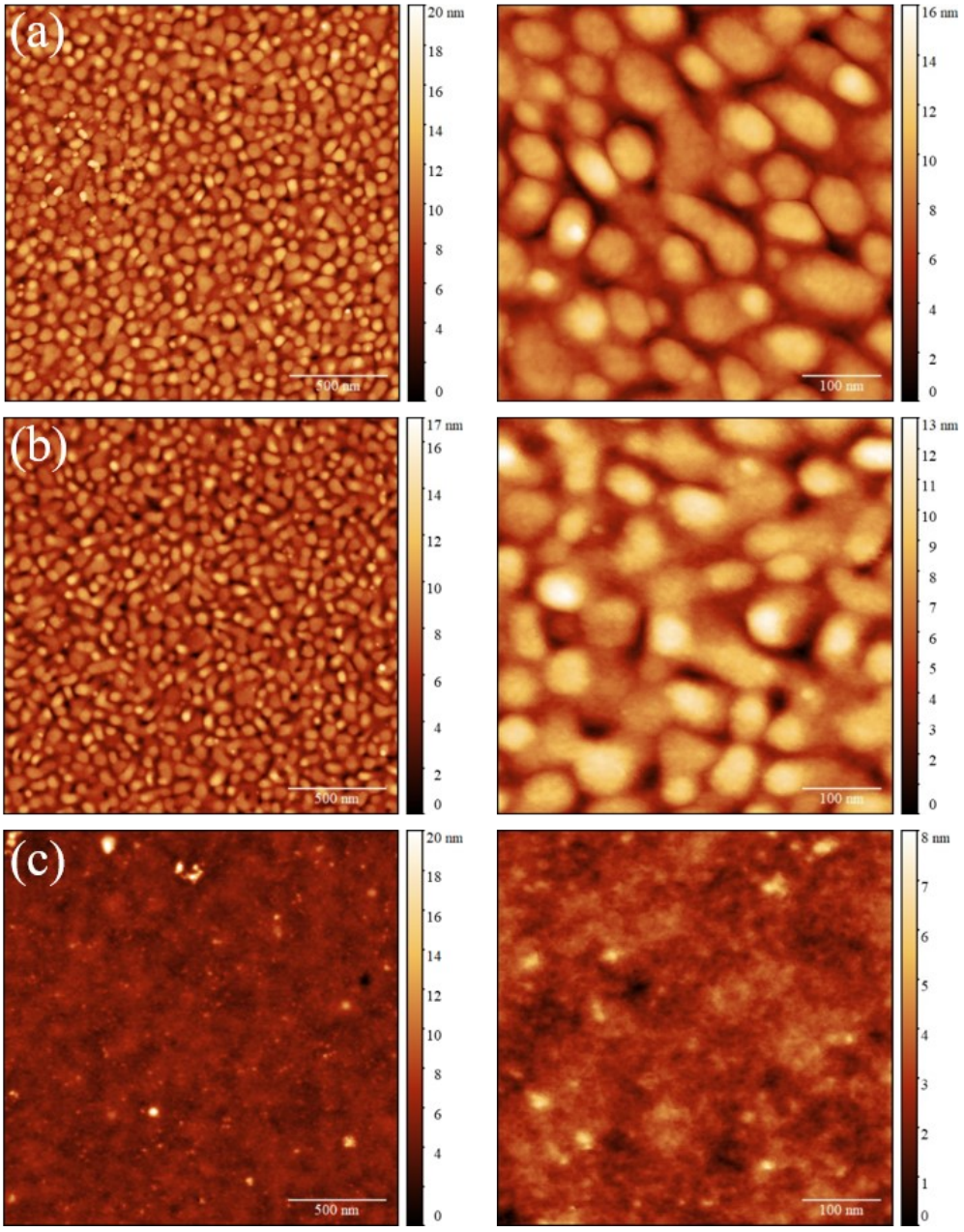

Fig. S2. AFM surface topography of (a) GT-GS-poly(HPMA) brushes on gold substrates, (b) GT-PS-poly(HPMA) brushes on gold substrates and (c) GF-poly(HPMA) brushes on silicon substrates. The measured root-mean-squared roughness of the poly(HPMA) brushes did not exceed 2 nm.

Analysis of SMFS data using the worm-like chain (WLC) model

The force-distance curves showing rupture events (Fig. S3) were fitted using the WLC model:

$$f(x) = \frac{k_b T}{l_p}\left[\frac{1}{4\left(1-\frac{x}{l_c}\right)^2} - \frac{1}{4} + \frac{x}{l_c}\right],$$

where x is the displacement length between AFM tip to the surface, f is the pull-off force, k_b is Boltzmann constant, T is the absolute temperature, l_p is the persistence length and l_c is the contour length.[1, 2] The number-average persistence length of GF-poly(HPMA) brushes of 13.5 ± 0.2 nm thickness was determined to be 0.17 ± 0.02 nm, while their number-average contour length was 67.2 ± 0.9 nm. The corresponding molar mass of GF-poly(HPMA) (Fig. S4) was calculated by dividing the number-average contour length by the size of repeat monomer unit (C–C–C bonds along the main chain, i.e. 2.73 Å).

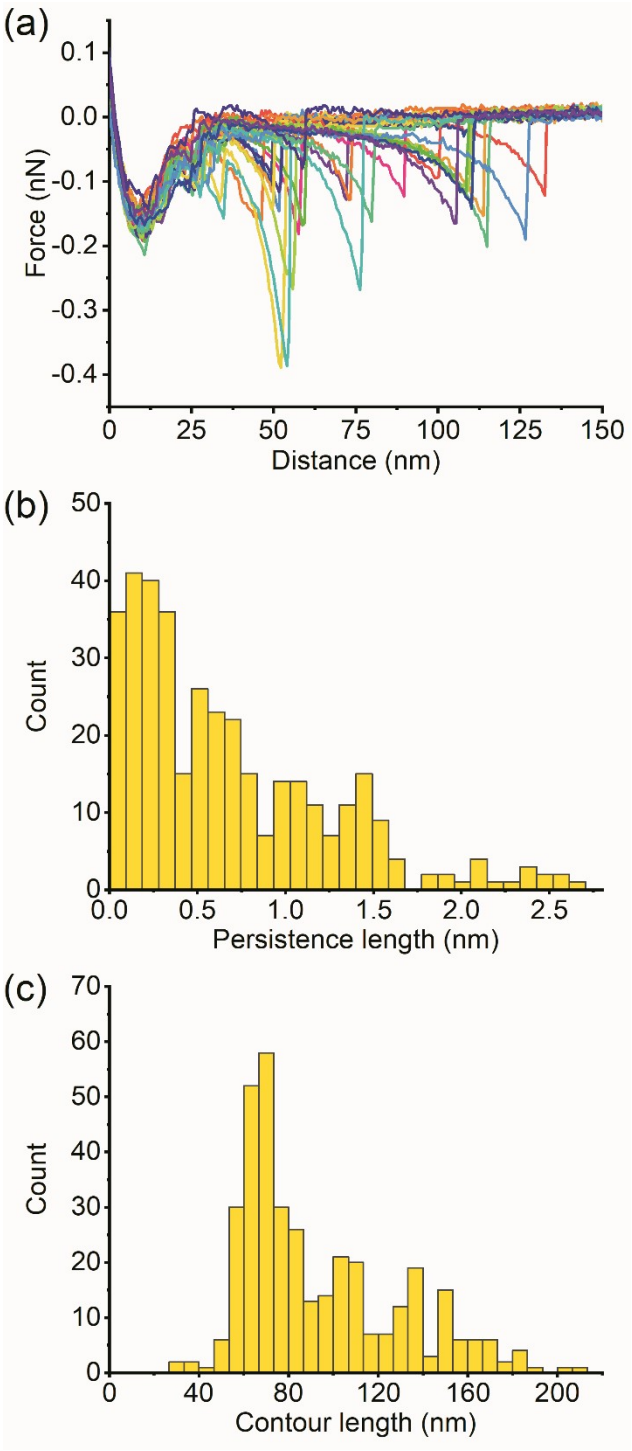

Fig. S3. Characteristic retraction force curves measured on thiol-terminated GF-poly(HPMA) brushes showing clear unfolding and rupture events (a). Distributions of persistence (b) and contour (c) lengths obtained from the fits of the pull-off forces using the WLC model.

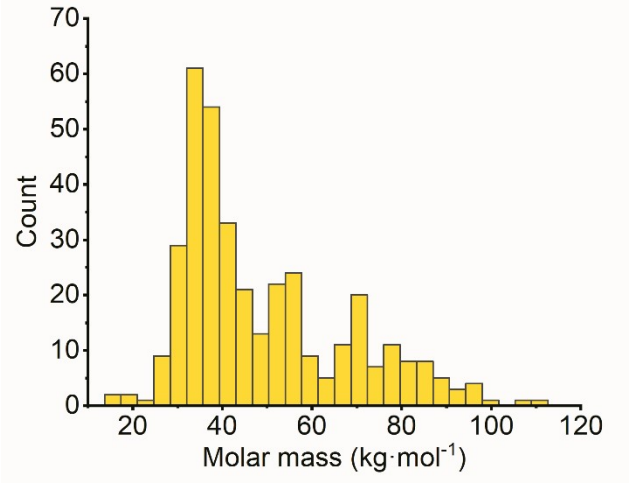

Fig. S4. Distribution of molar mass of GF-poly(HPMA) brushes obtained from the SMFS analysis.

Characterization of CTA self-assembled monolayers for SI-RAFT via XPS

SI-RAFT polymerization was employed for the synthesis of poly(HPMA) via GF method utilizing self-assembled monolayers bearing CTA moieties. The chain transfer agent was immobilized on a self-assembled monolayer bearing a tertiary bromine atom (Br-SAM). The bromine could be easily replaced in a one-step reaction following the atom transfer radical addition process to exchange with RAFT agent.[3] The successful immobilization of CTA group was confirmed by XPS. The C 1s region of the XPS spectrum of the Br-SAM surface presents contributions of C-C and C-H (285.0 eV), C-O and C-Br (286.6 eV), O-C=O (289.3 eV) and characteristic C-Br contributions in Br 3d region (spin–split Br $3d_{5/2}$–Br $3d_{3/2}$ doublet components centered at 70.3 eV and 71.3 eV, respectively) (Fig. S2 and Table S2). The exchange of bromine for the phenylcarbonothioylthio CTA moieties led to decreased C-Br contributions and a rise of new S-C(=S) contributions in S 2p region (spin–split S $2p_{3/2}$–S $2p_{1/2}$ doublet components centered at 163.3 eV and 164.6 eV, respectively (Fig. S2 and Table S2).

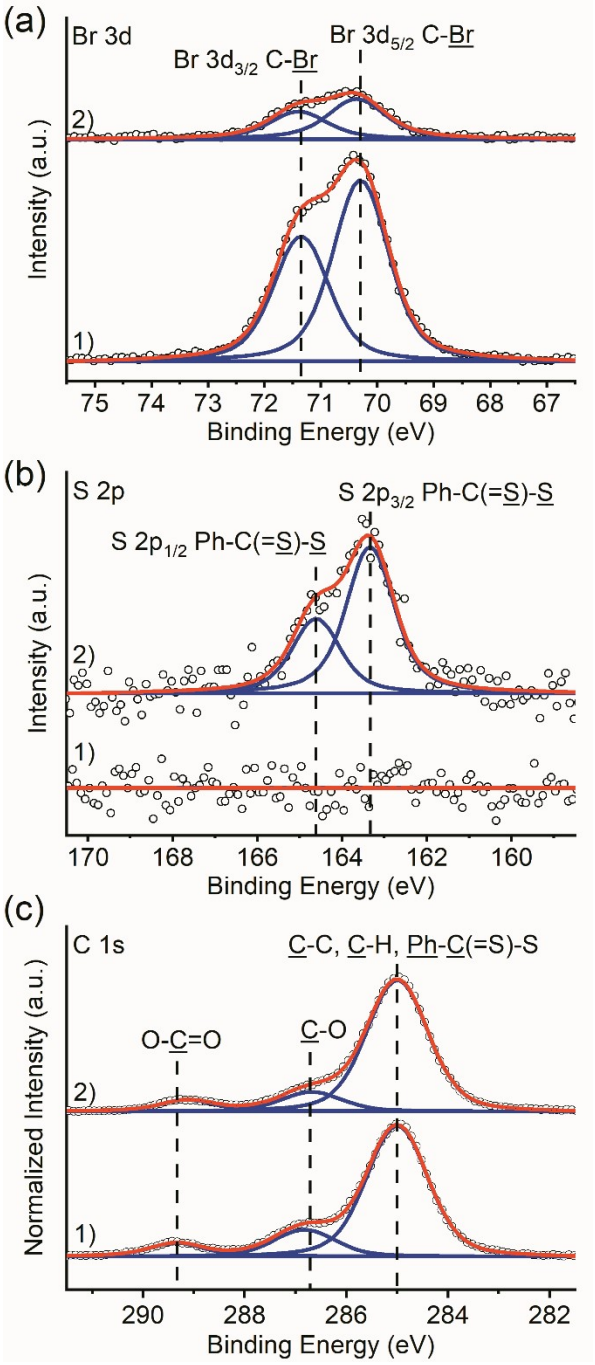

Fig. S5. XPS proves the immobilization of CTA on Br-SAM for GF method. High-resolution XPS spectra of (a) Br 3d, (b) S 2p and (c) C 1s regions for the Br-SAM (1) and CTA-SAM (2).

Note: Measured high-resolution spectra of Br 3d, S 2p and C 1s regions are presented with open circles, while their corresponding fitted envelopes are presented with red lines. The individual contributions of different functional groups (C 1s) and the spin–split doublet components (Br 3d and S 2p) are represented with blue lines.

Characterization of aminolysis reaction of GF-poly(HPMA)-CTA via XPS

The CTA end groups in the GF-poly(HPMA) brushes were converted to thiol (GF-poly(HPMA)-SH) by aminolysis before SMFS measurements in order to maximize binding with the gold-coated AFM cantilever tip. The high-resolution XPS spectra in the C 1s region proved the preserved structure of the poly(HPMA) brush (Fig. S3). Furthermore, the drop of the sulphur contributions upon the aminolysis reaction of GF-poly(HPMA)-CTA brushes (Table S2), and concomitant SEC-MALLS and NMR observations on bulk polymer (see further sections) pointed to the successful removal of CTA and thiol left as the polymer end group.

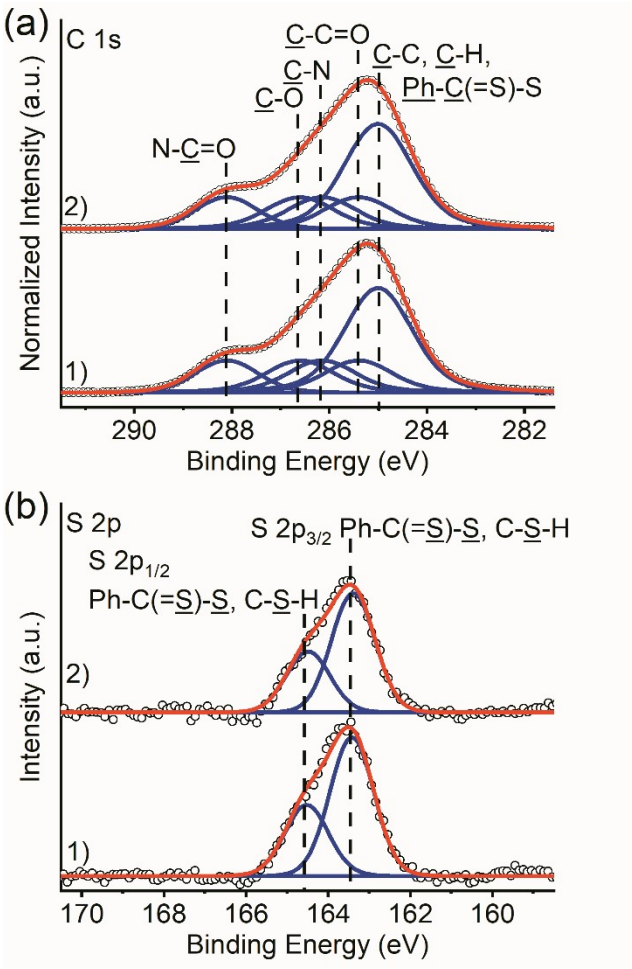

Fig. S6. XPS proves the preserved chemical structure of the GF-poly(HPMA) brush and points to the successful aminolysis of CTA to thiol at the distal chain end before SMFS measurements. High-resolution XPS spectra of (a) C 1s and (b) S 2p regions for the GF-poly(HPMA)-CTA (1) and GF-poly(HPMA)-SH (2).

Note: Measured high-resolution spectra of C 1s and S 2p regions are presented with open circles, while their corresponding fitted envelopes are presented with red lines. The individual contributions of different functional groups (C 1s) and the spin–split doublet components (S 2p) are represented with blue lines.

Characterization of covalent binding of GT-poly(HPMA) brushes by XPS

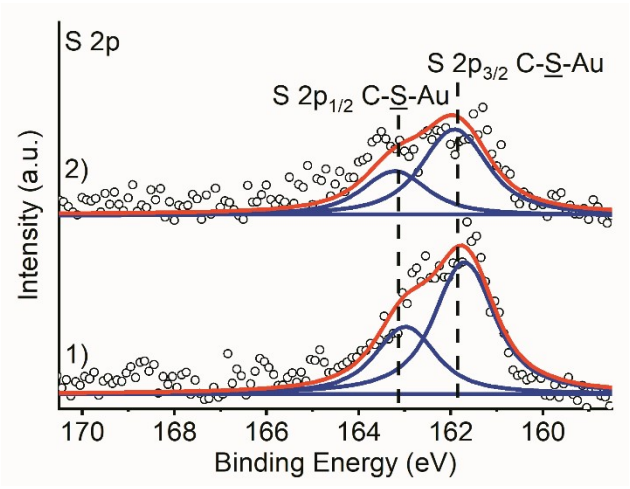

Fig. S7. XPS analysis proves the covalent binding of GT-poly(HPMA) to gold by GS (1) and PS (2) solutions through the establishment of C-S-Au bonds.

Note: Measured high-resolution spectra of S 2p region of poly(HPMA) brushes performed by GT-GS and GT-PS methods are presented with open circles, while their corresponding fitted envelopes are presented with red lines. The spin–split doublet contributions (S 2p) are represented with blue lines.

Table S2. Surface composition (%) of modified surfaces as determined by XPS.

Surfaces	C 1s C-C, C-H, Ph-C(=S)-S	C 1s C-C(=O)	C 1s C-N	C 1s C-O	C 1s N-C=O	C 1s O-C=O	N 1s N-C=O	O 1s	Br 3d5 C-Br	S 2p3 Ph-C(=S)-S, C-S-H, C-S-Au	Si 2p Si	Si 2p SiO_2	Au 4f7
Br-SAM	23.8			4.9		2.7		32.9	1.4		25.6	8.8	
CTA-SAM	27.9			4.1		2.6		29.9	0.3	0.8	26.7	7.7	
GT-GS-poly(HPMA)	20.3	7.3	7.3	7.3	7.3		7.5	14.1		2.7			26.1
GT-PS-poly(HPMA)	23.0	8.9	8.9	8.9	8.9		10.4	15.9		1.6			13.4
GF-poly(HPMA)-CTA	30.5	9.7	9.7	9.7	9.7		9.8	18.8		0.6	1.1	0.4	
GF-poly(HPMA)-SH	30.6	9.5	9.5	9.5	9.5		9.7	19.2		0.5	1.3	0.4	

Note: The surfaces of Br-SAM, GT-GS-poly(HPMA), GT-PS-poly(HPMA) and GF-poly(HPMA)-SH have no C 1s contribution of Ph-C(=S)-S. The surfaces of GT-GS-poly(HPMA), GT-PS-poly(HPMA) and GF-poly(HPMA)-SH have no S 2p contribution of Ph-C(=S)-S.

Characterization of aminolysis via SEC-MALLS and NMR

The poly(HPMA) synthesized by RAFT polymerization was collected from the solution and was measured by SEC-MALLS and NMR (Bruker Avance III spectrometer operating at 300.13 MHz (^{1}H) in d-DMSO) before and after the aminolysis reaction (chemical shifts were referenced to the residual solvent peak of d-DMSO at 2.50 ppm). Beside the unchanged molar mass of poly(HPMA), the SEC-MALLS analysis recorded decreased UV absorbance at 305 nm characteristic of the CTA moiety (Fig. S8). For NMR characterization of the aminolysis product, poly(HPMA) of M_n 17.0 kg·mol^{-1} was used (instead of M_n 49.0 kg·mol^{-1}) as it has a higher relative concentration of CTA end groups, enabling more precise monitoring of their disappearance. The aminolysis of the CTA chain end group of poly(HPMA) was supported by the disappearance of the phenyl group at 7.5–8.0 ppm (Fig. S6). Thus the SEC-MALLS and NMR observations point to the preserved chemical structure and molar mass of poly(HPMA) after the aminolysis reaction. (*Note:* Reduction reaction ($NaBH_4$ in methanol solution) was also attempted to convert the CTA into thiol (-SH) end group. Despite the fact that this reaction efficiently reduced the CTA chain end groups to thiols, it led to significant cleavage (more than 60%) of the GF-poly(HPMA) brushes. Therefore, we utilized the aminolysis reaction for the reduction of the CTA into thiol throughout this work).

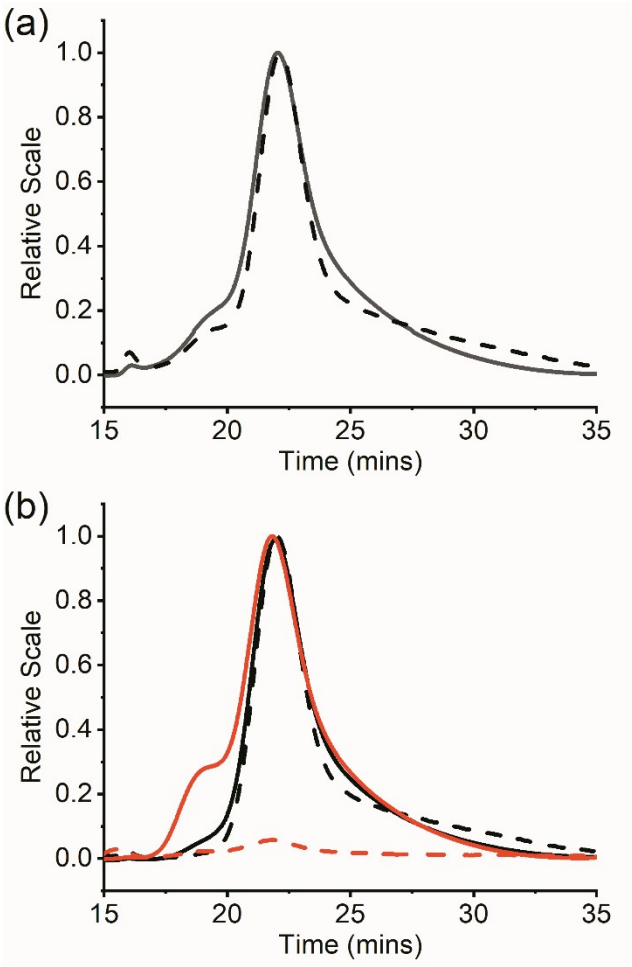

Fig. S8. SEC-MALLS chromatograms of poly(HPMA) (solid line: differential refractive index detector, dash line: UV detector). (a) Poly(HPMA) collected in solution during (SI-)RAFT (M_n = 47 kg·mol^{-1} with a $Đ$ = 1.46). (b) Poly(HPMA) (M_n = 49 kg·mol^{-1} with a $Đ$ = 1.18) prepared by RAFT polymerization for GT method before (black) and after aminolysis (red).

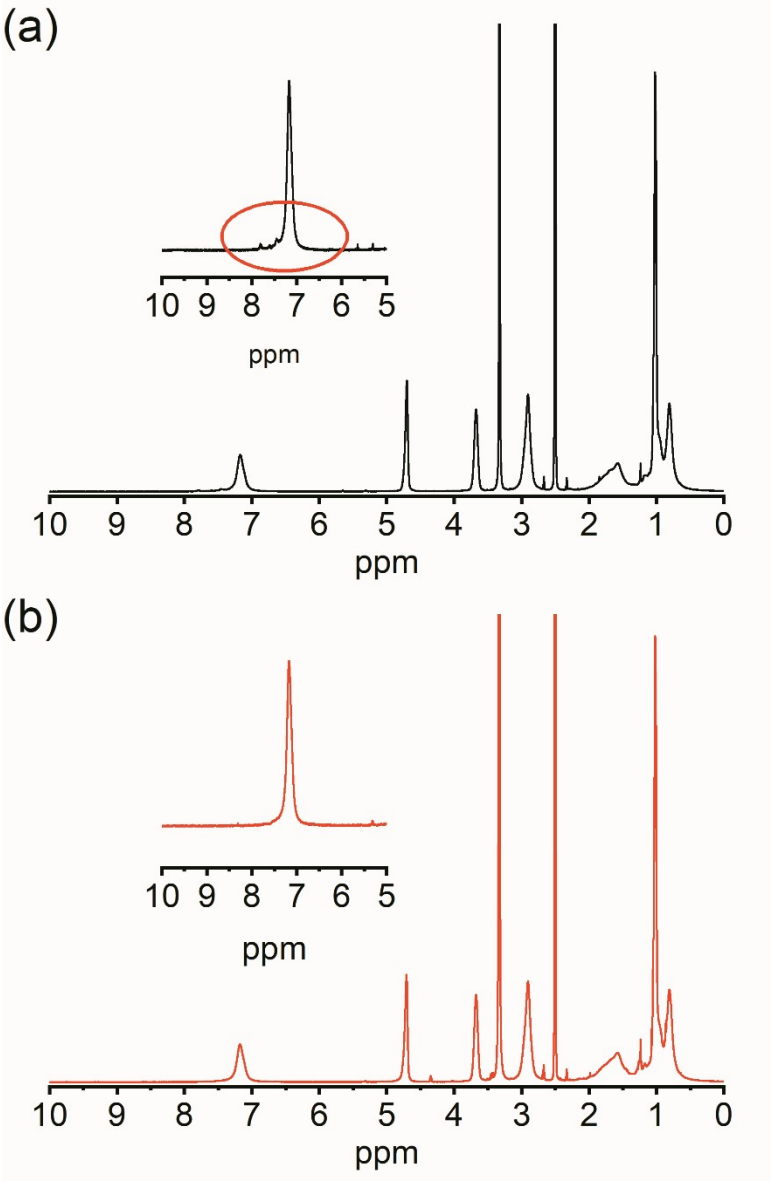

Fig. S9. ^{1}H NMR spectra of (a) poly(HPMA)-CTA and (b) poly(HPMA)-SH in d-DMSO. ***Note:*** The molar mass of poly(HPMA) presented here is M_n 17.0 kg·mol^{-1} instead of M_n 49.0 kg·mol^{-1} because of the relatively low proton integral value of phenyl group of CTA moiety to be observed at 7.5- 8 ppm for the disappearance.

Characterization of GT-poly(HPMA) and GF-poly(HPMA) by Fourier-transform infrared spectroscopy (FTIR)

FTIR measurements in reflection mode were performed on dry poly(HPMA) layers utilizing a Nicolet Nexus 870 FTIR spectrometer (ThermoFisher Scientific, USA) equipped with a grazing angle attenuated total reflection (GAATR; Ge hemispherical crystal, AOI range of 60–65°, VariGATR, Harrick Scientific Products, USA) and a grazing angle specular reflection (GASR; SAGA, ThermoFisher Scientific, USA) attachment. The measurement chamber of the spectrometer was continuously purged with dry air. Silicon substrates bearing poly(HPMA) brushes synthesized by GF methods were measured in the GAATR-FTIR mode, whereas the brushes synthesized by GT methods on gold substrates were measured in the GASR-FTIR mode. All spectra were acquired with 256 scans at a resolution of 2 cm^{-1} and processed with OMNIC software. The total acquisition time was about 3 min per spectrum. All reported FTIR spectra are presented as absorbance measured against reference spectra of freshly cleaned silicon and gold substrates.

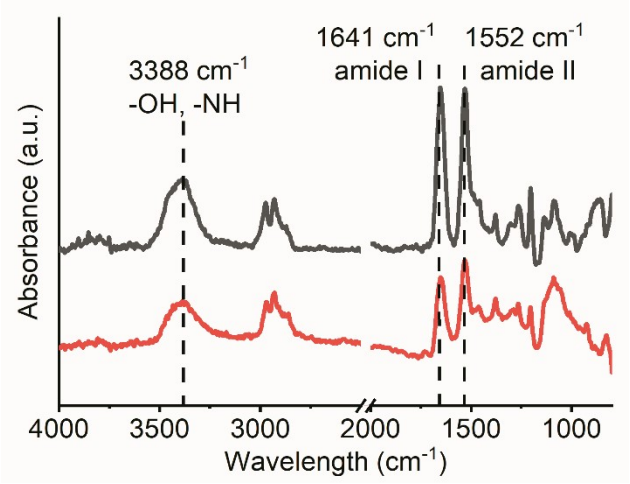

Fig. S10. GASR-FTIR spectra of GT-poly(HPMA) brushes synthesized by GS (red) and PS (black) conditions on gold substrates.

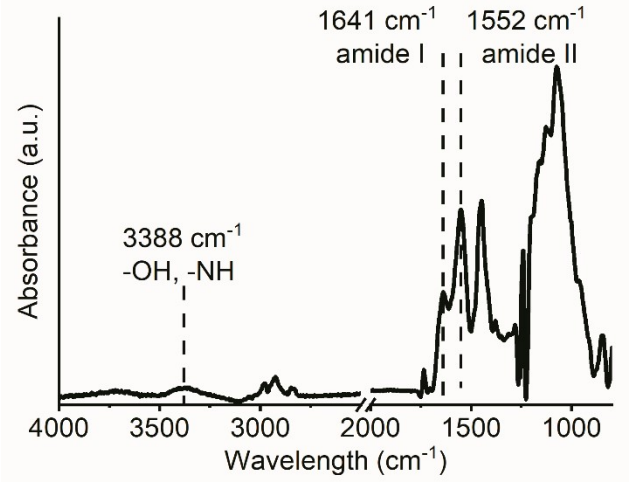

Fig. S11. GAATR-FTIR spectra of GF-poly(HPMA) brushes on silicon substrates.

Fouling resistance of poly(HPMA) coatings prepared by GT and GF method

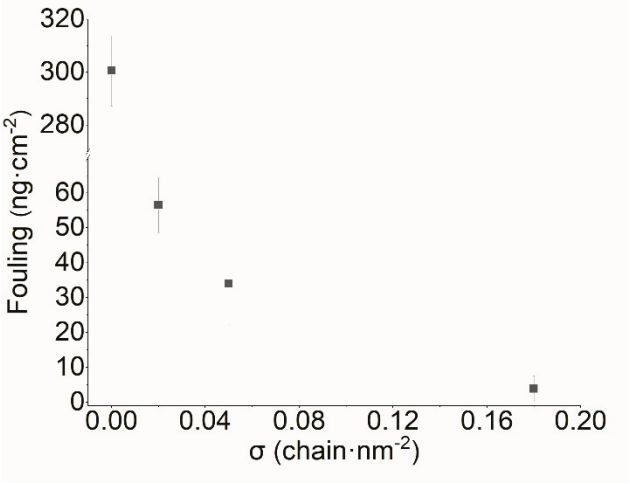

Fig. S12. Dependence of resistance to fouling from HBP with increasing grafting densities of poly(HPMA) brushes.

References

1. C. Bouchiat, M. D. Wang, J. F. Allemand, T. Strick, S. M. Block and V. Croquette, *Biophys. J.*, 1999, **76**, 409-413.
2. T. Tischer, R. Gralla-Koser, V. Trouillet, L. Barner, C. Barner-Kowollik and C. Lee-Thedieck, *ACS Macro. Lett.*, 2016, **5**, 498-503.
3. Y. Tsujii, M. Ejaz, K. Sato, A. Goto and T. Fukuda, *Macromolecules*, 2001, **34**, 8872-8878.